

tion, the pathway may not be sufficient to unambiguously specify polarity in other organs such as heart and spleen, resulting in heterotaxia. In any case, the *inv* mutation provides a new model system for studies on the specification of left-right polarity during vertebrate development.

REFERENCES AND NOTES

1. K. P. Hummel and D. B. Chapman, *J. Hered.* **50**, 10 (1959).
2. W. M. Layton, *ibid.* **67**, 336 (1976).
3. M. Kartagener and A. Horlacher, *Schweiz. Med. Wochenschr.* **65**, 782 (1935).
4. J. Torgeson, *Arch. Pathol.* **47**, 566 (1949).
5. M. J. Morgan, in *Biological Asymmetry and Handedness*, G. R. Bock and J. Marsh, Eds. (Wiley, Chichester, United Kingdom, 1991), pp. 234–250.
6. T. Yokoyama *et al.*, *Nucleic Acids Res.* **18**, 7293 (1990).
7. T. Yokoyama and P. A. Overbeek, unpublished results.
8. B. A. Afzelius, *Science* **193**, 317 (1976).
9. W. Brinkley, personal communication.
10. Large molecular weight DNA was isolated from 3-day-old mutant mouse kidney as described (11). The DNA was digested partially with *Sau* 3AI; fragments larger than 15 kb were isolated by fractionation on a sucrose gradient (12) then ligated to the Lambda EMBL3 vector (Stratagene) that had been digested with *Bam* HI. Ligation products were packaged in vitro with Gigapack II (Stratagene). Approximately 5×10^5 plaques were screened with the tyrosinase minigene TyBS (6) as a probe. Positive plaques were purified through three rounds of screening then assayed for the presence of tyrosinase cDNA sequences with the use of the polymerase chain reaction (6). Genomic sequences from the λ clones were subcloned and tested for single-copy sequences by Southern hybridization (13).
11. J. L. Longmire, K. L. Albright, A. K. Lewis, L. J. Meincke, C. E. Hildebrand, *Nucleic Acids Res.* **15**, 859 (1987).
12. J. H. Weis, in *Current Protocols in Molecular Biology*, F. M. Ausubel *et al.*, Eds. (Wiley, New York, 1987), 5.3.2–5.3.8.
13. R. F. Seldon, *ibid.*, 2.9.1–2.9.10.
14. N. G. Copeland and N. A. Jenkins, *Trends Genet.* **7**, 113 (1991).
15. DNA isolation, restriction enzyme digestion, agarose gel electrophoresis, Southern blot transfer, and hybridization were performed essentially as described (16). The *inv* genomic probe (p3.2H) (Fig. 2A) was labeled with [α - 32 P]deoxycytidine 5'-triphosphate (dCTP) with a nick translation labeling kit (Boehringer Mannheim). A 9.6-kb fragment was detected in *Bam* HI-digested C57BL/6J DNA and 6.6- and 3.7-kb fragments were detected in *Bam* HI-digested *M. spretus* DNA. The 6.6- and 3.7-kb *M. spretus*-specific fragments cosegregated and were followed in backcross mice.
16. N. A. Jenkins, N. G. Copeland, B. A. Taylor, B. K. Lee, *J. Virol.* **43**, 26 (1982).
17. M. Brueckner, L. A. D'Hoostelaere, A. Calabro, P. D'Eustachio, *Proc. Natl. Acad. Sci. U.S.A.* **86**, 5035 (1989).
18. N. A. Brown, A. McCarthy, L. Wolpert, in (5), pp. 182–201.
19. K. Theiler, in *The House Mouse: Atlas of Embryonic Development* (Springer-Verlag, New York, 1989), pp. 40–42.
20. W. M. Layton and F. J. Manasek, in *Etiology and Morphogenesis of Congenital Heart Disease*, R. Van Praugh and A. Takao, Eds. (Futura, Mount Kisco, NY, 1980), pp. 109–128.
21. N. A. Brown and L. Wolpert, *Development* **109**, 1 (1990).
22. M. J. Morgan and M. C. Corballis, *Behav. Brain Sci.* **2**, 270 (1978).
23. H. J. Yost, *Nature* **357**, 158 (1992).
24. J. D. Ceci, L. D. Siracusa, N. A. Jenkins, N. G. Copeland, *Genomics* **5**, 699 (1989).
25. C.-L. Hsieh, U. Dorries, M. Schachner, U. Franke, *Mammalian Genome* **1**, S522 (1991).
26. E. L. Green, *Genetics and Probability in Animal Breeding Experiments*, (Oxford Univ. Press, New York, 1981), pp. 77–113.
27. A. P. Feinberg and B. A. Vogelstein, *Anal. Biochem.* **137**, 266 (1984).
28. The ratios of the total number of mice that exhibited recombinant chromosomes to the total number of mice analyzed for each pair of loci and the most likely gene order are: centromere-*Mos* (9/122) *Tsha* (7/121) *inv* (19/190) *Hxb*. The recombination frequencies (expressed as genetic distances in centimorgans \pm SE) are: *Mos* (7.4 ± 2.4) *Tsha* (5.8 ± 2.1) *inv* (10.0 ± 2.2) *Hxb*. Descriptions of the probes and restriction fragment length polymorphisms for the loci linked to the *inv* locus, including *Mos* and *Tsha*, have been reported previously (24). One locus used to position *inv* on chromosome 4 has not been reported previously for our interspecific map. The probe for the *Hxb* locus was a 2-kb mouse cDNA from the 3' end of the gene (25) that detected 7.0-, 6.4-, 5.8-, 1.2-, and 1.0-kb fragments in *Pvu* II-digested C57BL/6J DNA and 9.0-, 6.4-, 5.6-, 1.4-, 1.2-, and 1.0-kb fragments in *Pvu* II-digested *M. spretus* DNA. The 9.0-kb *M. spretus*-specific fragment was followed in this analysis. Recombination distances were calculated as described (26) with the computer program SPRETUS MADNESS (unpublished program). We determined the gene order by minimizing the number of recombination events required to explain the allele distribution patterns.
29. We wish to thank R. Collins for providing the Sl/Col mice, W. Brinkley and D. Turner of the Cell Biology Microscopy Core Laboratory for electron microscopy, R. Geske for help with photography and histology, L. Kairewich for artistic assistance, D. J. Gilbert for excellent technical assistance, T. Reid for help with the manuscript, and G. MacGregor for critical reading of the manuscript. This research was supported, in part, by NIH grant HD25340 (P.A.O.) and by the National Cancer Institute, Department of Health and Human Services, under contract NO1-CO-74101 with ABL. All mice used in this study were handled in accordance with the NIH Guide for the Care and Use of Laboratory Animals with protocols approved by the Animal Protocol Review Committee of the Baylor College of Medicine.

1 December 1992; accepted 22 March 1993

Cytoskeletal Role in the Contractile Dysfunction of Hypertrophied Myocardium

Hiroyuki Tsutsui,* Kazuaki Ishihara,† George Cooper IV‡

Cardiac hypertrophy in response to systolic pressure loading frequently results in contractile dysfunction of unknown cause. In the present study, pressure loading increased the microtubule component of the cardiac muscle cell cytoskeleton, which was responsible for the cellular contractile dysfunction observed. The linked microtubule and contractile abnormalities were persistent and thus may have significance for the deterioration of initially compensatory cardiac hypertrophy into congestive heart failure.

Cardiac hypertrophy is the response to many physiological and pathological deviations from normal homeostasis that have in common increased hemodynamic loading of the heart (1). This growth process proceeds until the load stimulus is abated by way of a renormalization of stress per unit of myocardial mass. Hypertrophy fails to be functionally compensatory when either the load increase exceeds the growth capacity of the terminally differentiated cardiac muscle cell (or cardiocyte) to renormalize stress or when the contractile performance per unit mass of hypertrophied myocardium is less than that of normal myocardium. Thus, cardiac compensation for an increased load

may be imperfect because of either quantitative or qualitative defects of hypertrophied myocardium.

This study investigated the qualitative defects of hypertrophied myocardium, which may underlie the frequent deterioration of initially compensatory cardiac hypertrophy into congestive heart failure. Hemodynamic overloads causing cardiac hypertrophy consist of either (i) volume overloading, in which an increased blood volume is pumped during each cardiac cycle against a normal impedance, or (ii) pressure overloading, in which a normal blood volume is pumped during each cardiac cycle against an increased impedance. In tissue from the volume-overloaded right ventricle, normal cardiac mechanics are maintained (2), whereas pressure overloading produces distinctly abnormal cardiac mechanics on both the tissue (3) and cardiocyte (4) levels. Thus, the nature of the stress rather than hypertrophy itself causes the qualitative defects of myocardium hypertrophying in response to a pressure overload, and the contractile defect lies in the cardiocyte.

Although potential causes for the abnor-

H. Tsutsui, K. Ishihara, G. Cooper IV, Gazes Cardiac Research Institute, Cardiology Division, Department of Medicine and Department of Physiology, Medical University of South Carolina and the Veterans Administration Medical Center, Charleston, SC 29401.

*Present address: Research Institute of Angiocardiology and Cardiovascular Clinic, Kyushu University School of Medicine, 3-1-1 Maidashi, Higashi-ku, Fukuoka, 812, Japan.

†Present address: Department of Pediatric Cardiovascular Surgery, Heart Institute of Japan, Tokyo Women's Medical College, 8-1 Kawada-cho, Shinjuku-ku, Tokyo, 162, Japan.

‡To whom correspondence should be addressed.

malities of hypertrophied myocardium have been evaluated (1, 3, 5), none accounts fully for either the contractile abnormalities of hypertrophied myocardium or for the differences observed in the pressure versus volume-overloaded right ventricle. We therefore sought the cause for the contractile defect by studying intracellular structures that might (i) appear or increase in response to load, (ii) discriminate between the stimuli of stress or pressure loading versus strain, or volume loading, (iii) not be obvious ultrastructurally, and (iv) be thought to have the potential for interfering with sarcomere motion.

We tested the hypothesis that in excess, the cytoskeletal microtubules are responsible for the contractile abnormalities of cardiocytes hypertrophying in response to a pressure overload. The basis for this hypothesis by the four criteria above is as follows: (i) In taxa as diverse as plants (6), invertebrates (7), and vertebrates (8) microtubules form along intracellular and transcellular stress axes, suggesting polymerization or organization in response to the mechanical environment. (ii) For a linear steady-state polymer such as the $\alpha\beta$ -tubulin heterodimer-microtubule system, thermodynamics dictate that the critical subunit concentration for assembly is lowered and polymer stability is enhanced by an extending, or stress, force (9), and there is evidence that this obtains for microtubules in growing axons (10). (iii) Whereas there are neither qualitative nor quantitative ultrastructural differences between hypertrophied cardiocytes from pressure versus volume-overloaded right ventricles (11), microtubules are not obvious by standard ultrastructural analysis in mature striated muscle. (iv) Given the intimate cardiac myofibrillar investment by microtubules (12), in excess they might interfere with sarcomere motion.

Right ventricular (RV) pressure overload or RV volume overload were produced in adult cats of either sex by pulmonary artery banding or atrial septotomy, respectively (13). For the pressure overload model, RV systolic pressure was doubled, and there was a 39% increase in the ratio of RV to body mass. For the volume overload model, a significant left-to-right shunt was present at the atrial level, and there was a 56% increase in the ratio of RV to body mass. Cellular surface area of RV cardiocytes (14) increased by 22% in pressure overload and 21% in volume overload (Table 1).

Microtubule density was estimated from laser scanning confocal images of RV and left ventricular (LV) cardiocytes immunolabeled with an antibody to β -tubulin. A quantitative estimate of the free and polymerized pools of tubulin in RV and LV myocardium was made with this antibody in

protein immunoblots (Fig. 1). For the control and the atrial septal defect (ASD) cats, microtubule density appeared equivalent in the RV and LV cardiocytes. The immunoblots showed equivalent amounts and proportions of free and polymerized β -tubulin in the RV and LV myocardium. For the pulmonary artery band (PAB) cats at both 2 weeks and 4 weeks, the LV micrographs and immunoblots were equivalent to those from the RV and LV samples from control and ASD cats. However, the RV micrographs and immunoblots were quite different. The micrographs showed an increased microtubule density in the RV cells, and the immunoblots showed an increase in both free and polymerized β -tubulin in the RV myocardium. A quantitative analysis

was done of five blots from each of these four groups in which bovine brain β -tubulin was run with the unknowns in order to construct a standard curve (10). Free, polymerized, and total β -tubulin were each approximately doubled in the RV samples from the two PAB groups, and one-third (30 to 35%) of the β -tubulin was polymerized in both the RV and the LV myocardium of all groups. Thus, microtubules as well as free β -tubulin were selectively increased in myocardium hypertrophying in response to a stress overload.

Exposure of hypertrophied RV cardiocytes from 2-week PAB cats to colchicine largely normalized the initially abnormal contractile function (Fig. 2). Sarcomere motion and its first derivative did not

Table 1. Characteristics of the pressure overload and volume overload models. ASD, atrial septal defect (volume overload); PAB, pulmonary artery band (pressure overload); RV, right ventricle; SVC, superior vena cava; RA, right atrium; *n*, number of cats. For the ASD (2 weeks and 4 weeks) and PAB (2 weeks, 4 weeks, and 6 months) cats, there was no within-group difference for any of these variables at the various experimental time points; the data for all such times within each of these groups are therefore treated together in this table. Controls consisted of either normal cats or sham-operated cats submitted to thoracotomy and pericardiectomy without hemodynamic intervention. Because sham operation had no effect on any experimental variable, all control cats are considered as a single group. There was no evidence for congestive heart failure in any group in terms of increased body mass, arteriovenous O₂ difference, RV end-diastolic pressure, or ratio of liver mass to body mass. Values are given by the mean \pm SEM. Statistical comparisons are by one-way ANOVA followed by Neuman-Keuls *t* test (33).

	Control (<i>n</i> = 14)	ASD (<i>n</i> = 10)	PAB (<i>n</i> = 27)
RV systolic pressure (mm Hg)	25.7 \pm 1.5	28.3 \pm 1.3	53.9 \pm 1.3*†
Δ O ₂ percent saturation (SVC versus RA)	-0.5 \pm 0.6	9.5 \pm 1.6*	0.6 \pm 0.6†
RV mass/body mass (g/kg)	0.59 \pm 0.04	0.92 \pm 0.11*	0.82 \pm 0.02*
RV cardiocyte surface area (μ m ²)	2699 \pm 107	3267 \pm 122*	3294 \pm 44*

**P* < 0.01 for difference from control. †*P* < 0.01 for difference from ASD.

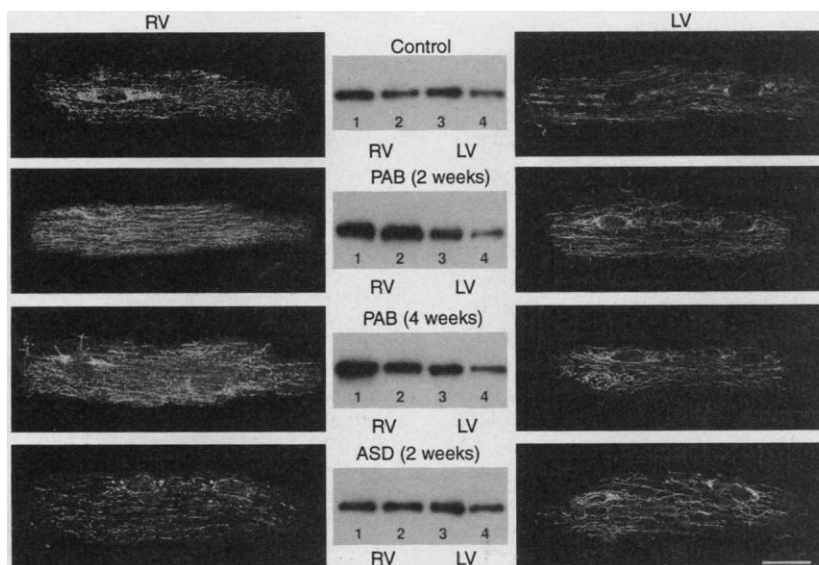


Fig. 1. Immunoblot analysis of free (lanes 1 and 3) and polymerized (lanes 2 and 4) tubulin in myocardium and immunofluorescence micrograph analysis of microtubules in isolated cardiocytes (37). Lanes 1 and 2 and the corresponding micrographs are from the right ventricle; lanes 3 and 4 and the corresponding micrographs are from the left ventricle. PAB, pulmonary artery band; ASD, atrial septal defect. The bar represents 25 μ m.

change noticeably during the sequential sampling of a single LV cell (Fig. 2A); however, the initially depressed extent and velocity of sarcomere shortening in an RV cell from the same heart improved in response to colchicine (Fig. 2B). The contractile function of RV and LV cardiocytes from 2-week PAB cats became statistically indistinguishable by 30 min after colchicine exposure (Fig. 2, C and D). In an identical study with RV and LV cardiocytes from 4-week PAB cats (15) [the time after pressure overloading at which abnormal myocardial as opposed to cellular contractile function was defined previously in this model (3)], the findings replicated those shown (Fig. 2) except that contractile function became both statistically and numerically equivalent in the hypertrophied RV and normal LV cardiocytes by 30 min after colchicine exposure. Sarcomere mechanics of RV and LV cardiocytes from control cats were identical (15).

To be significant in the transition from compensatory cardiac hypertrophy to decompensated cardiac failure, any abnormality of contractile function must be a persistent rather than transient feature of the hypertrophic growth process. The same study was thus repeated on an additional group of PAB cats at 6 months, a time remote from the induction of RV pressure overload. Cardiocyte contractile function as characterized by sarcomere motion was again quite abnormal at baseline in the hypertrophied RV cells, but both the extent and the velocity of sarcomere shortening became identical to those of LV cardiocytes from the same cats after 30 min of colchicine exposure (Fig. 3).

Our hypothesis suggests that the intracellular alteration that underlies the contractile dysfunction of myocardium hypertrophying in response to a pressure overload should not be present in myocardium hypertrophying for a comparable time and to a comparable extent in response to a volume overload—that is, the alteration should appear only in response to stress overloading. We thus repeated this study on two groups of ASD cats, where we have found contractile function on the myocardial level to be entirely normal (2). Contractile performance of RV and LV cardiocytes from 2- and 4-week ASD cats was identical at baseline and remained so during colchicine exposure (15). As with RV and LV cardiocytes from control cats, there was a modest and comparable but statistically insignificant increase in contractile function during colchicine exposure for cells from both groups.

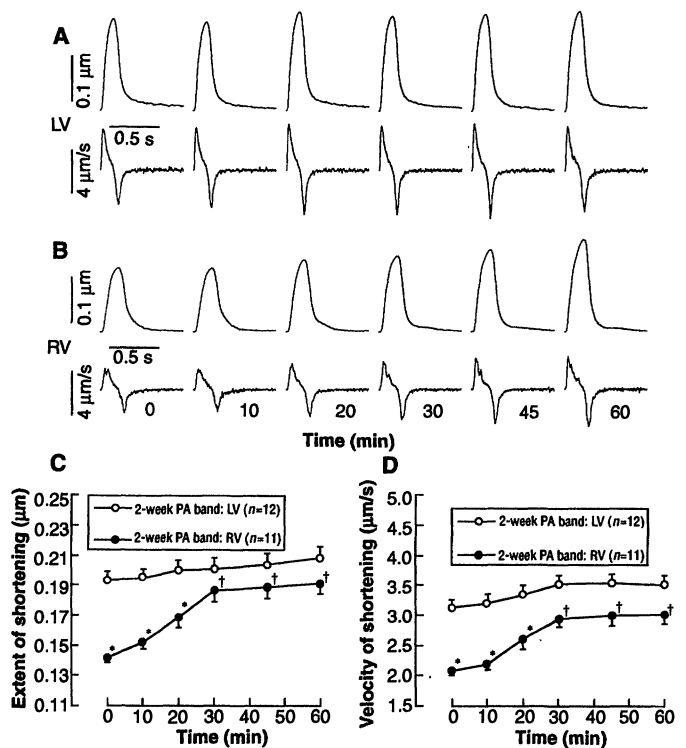
Colchicine affects the frequency but not the intensity of neonatal cardiocyte contractions (16, 17), but its effects on the mechanics of adult cells have not been

defined. For this reason and to exclude the possibility that the effects observed were unrelated to microtubule depolymerization, we examined sarcomere mechanics after depolymerizing cardiocyte microtubules by a quite different means. Because microtubules fully depolymerize on exposure to a temperature of 0°C for 1 hour but repolymerize on rewarming with an early time constant less than half of that for depolymerization (18), we cooled hypertrophied RV cardiocytes and normal LV cardiocytes from 2-week PAB cats to 0°C for 1 hour, followed by abrupt rewarming to 37°C. Sarcomere motion was defined before cooling, at rewarming before microtubule repolymerization was detectable, and after a further hour at 37°C when microtubule repolymerization was apparently complete. When cardiocytes from these cats were kept at 37°C throughout the study period as a control, the initially normal contractile function of LV cardiocytes and abnormal contractile function of RV cardiocytes were maintained. When cardiocytes were first studied at 37°C (T0), studied again at 37°C after an intervening hour at 0°C (T1), and then studied again after a further hour at 37°C (T2), the initially abnormal contrac-

tile function of RV cardiocytes was normalized by T1, and contractile function was the same as that for LV cardiocytes at T2 (Fig. 4, A and B). Both RV and LV cardiocytes showed a modest decrement in contractile function during microtubule repolymerization between T1 and T2 similar in degree to the increase in contractile function seen for normal cardiocytes during microtubule depolymerization (Figs. 2 and 3). Of particular interest in the context of our hypothesis, when cardiocyte microtubules that polymerized under a stress load in vivo polymerized under zero load in vitro, the initial contractile abnormality did not recur (Fig. 4, A and B; RV T0 versus RV T2).

If an excess of microtubules causes the contractile dysfunction seen in cardiocytes hypertrophying in response to a pressure overload, excessive microtubule polymerization should cause the same contractile dysfunction in normal cardiocytes. Taxol lowers the critical concentration of $\alpha\beta$ -tubulin heterodimers required to form microtubules (19); thus, it may mimic the hypothesized effect of a stress load on the $\alpha\beta$ -tubulin heterodimer-microtubule system of cardiocytes. Sarcomere motion and its first derivative did not change noticeably

Fig. 2. Effects of colchicine on sarcomere motion in cardiocytes (32) isolated from cats submitted to RV pressure overloading by pulmonary artery banding 2 weeks previously. (A) Sequential samples from a single LV cardiocyte. For each contraction, sarcomere length versus time is given above, and the rate of length change versus time is given below. (B) Sequential samples from a single RV cardiocyte from the same cat as the cell shown in (A). For each contraction, sarcomere length versus time is given above, and the rate of this length change is given below. The time (in minutes) after the addition of colchicine is indicated. (C) Summary data for the maximum extent of sarcomere shortening (initial sarcomere length – minimum sarcomere length) at the indicated times after addition of colchicine to RV and LV cardiocytes from the same cats. All cells were sampled sequentially at each of the indicated times after drug exposure. (D) Summary data for the maximum velocity of sarcomere shortening (maximum positive rate of length change) for the same cells shown in (C). Resting sarcomere length was $1.93 \pm 0.02 \mu\text{m}$ for the LV cells versus $1.93 \pm 0.02 \mu\text{m}$ for the RV cells [$P = \text{not significant (NS)}$]. For (C) and (D), statistical comparisons are by two-way analysis of variance (ANOVA) and a means comparison contrast (33), where $n = \text{number of cells}$. * $P < 0.001$ for difference from the LV value at matched time points; † $P < 0.001$ for difference from the initial time 0 value within a group.



during the sequential sampling of portions of normal cardiocytes; however, the initially normal extent and velocity of sarcomere shortening decreased markedly during 3 hours of exposure to taxol and remained at this diminished level at 4 hours (Fig. 5, A and B). Thus, taxol caused the sarcomere motion of normal cardiocytes to mimic the abnormal sarcomere motion of cardiocytes hypertrophying in response to a stress load.

To confirm that the mechanical effects of taxol resulted from microtubule hyperpolymerization, we examined the mechanical effects of microtubule hyperpolymerization induced through a different mechanism by using deuterium oxide (D₂O), which is thought to reduce the critical concentration of $\alpha\beta$ -tubulin heterodimers required to form microtubules by rapidly and reversibly strengthening hydrophobic interactions of tubulin molecules (20). When 50% D₂O was substituted for H₂O in the superfusing buffer of normal cardiocytes, there was a 29% decrease in the extent of shortening and a 36% decrease in the velocity of shortening within 10 min; these effects were then fully reversed 10 min after resubstitution of 100% H₂O in the superfusing buffer.

Microtubule dissolution by colchicine alkaloids may also alter the normal architecture of intermediate filaments in fibroblasts, but hypothermic microtubule dissolution does not have this effect (21). To be certain that intermediate filament alterations did not produce the effects on cardiocyte contractile function described, cells from the

T0, T1, and T2 groups in Fig. 4 were prepared for laser scanning confocal microscopy with the use of a monoclonal antibody against desmin (as in Fig. 1). The clearly defined intermediate filament network was not altered either by cooling, which completely removed the microtubules, or by rewarming, which restored the microtubule appearance to normal (15). To assess the possible role of microfilament alterations in cardiocyte contractile dysfunction, we applied cytochalasin D at a concentration of 2 μ g/ml, which disrupts the cortical microfilaments of mature myotubes within 45 min (22), to RV and LV cells from control and 2-week PAB cats. No improvement in contractile function was observed over a period of 1 hour in any cell (15). This suggests that of the three major classes of cytoskeletal filaments, only the microtubules are causally involved in the contractile dysfunction of cardiocytes hypertrophying in response to a pressure overload.

The present study, as well as other studies in which we have found that in both normal and stress-hypertrophied cardiocytes, mechanical coupling between sarcomere and sarcolemma motion is unaltered by microtubule dissolution, even with extracellular loading (23), suggest that the microtubule component of the cytoskeleton imposes a resistive intracellular load on the shortening sarcomere rather than altering the stiffness of the sarcomere-sarcolemma connections. An excess of microtubules in stress-hypertrophied cells increases this load and impedes sarcomere motion. Increased

cardiocyte microtubule density had been observed only transiently during the onset of cardiac hypertrophy (24) or as a feature of a subset of degenerated cardiocytes from failing hearts (25). In contrast, we find that there is a persistent increase in polymerized tubulin in cardiocytes that hypertrophy in response to a stress overload.

The association of excessive microtubules with contractile dysfunction and the full reversibility of this dysfunction after microtubule depolymerization raise several

Fig. 3. Effects of colchicine on sarcomere motion in cardiocytes isolated from cats submitted to RV pressure overloading by pulmonary artery banding 6 months previously. The format for this figure, and the attendant methods, are identical to those given (Fig. 2). Resting sarcomere length was $1.93 \pm 0.03 \mu\text{m}$ for the LV cells versus $1.95 \pm 0.05 \mu\text{m}$ for the RV cells ($P = \text{NS}$). $*P < 0.001$ for difference from the LV value at matched time points; $\dagger P < 0.001$ for difference from the initial time 0 value within a group.

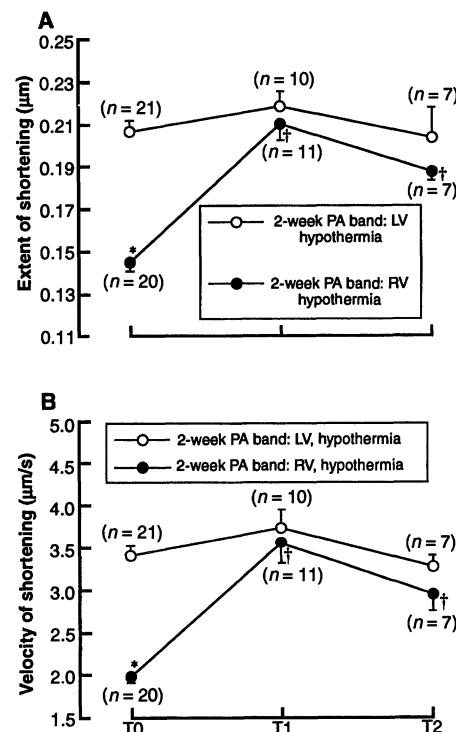
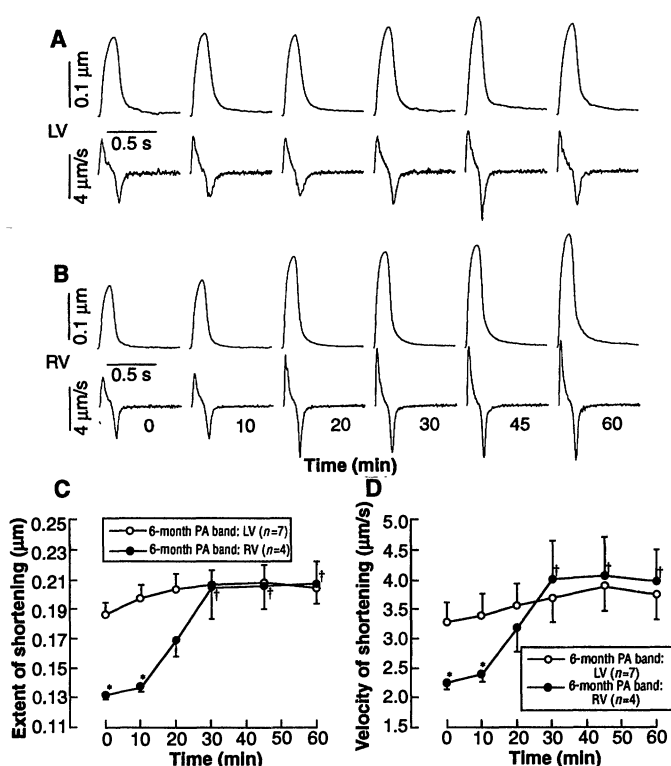


Fig. 4. Effects of cold on the maximum extent (A) and velocity (B) of sarcomere shortening in cardiocytes isolated from cats submitted to RV pressure overloading produced by pulmonary artery banding 2 weeks previously. Portions of RV and LV cells were first studied at 37.0°C (T0). The cells were then placed in 0°C buffer for 1 hour, after which cell portions were abruptly rewarmed by placement of 100- μ l samples in 4 ml of 37.0°C buffer in a chamber on the thermostated heating stage of the microscope, and then studied immediately (T1). Additional portions were studied after a further hour at 37.0°C (T2). Immunoblot analysis of free and polymerized tubulin and immunofluorescence micrograph analysis of microtubules in isolated cardiocytes, with the methods described (Fig. 1), demonstrated for the hypothermia cardiocytes an absence of microtubules at T1 and a normal complement of microtubules at T2 (15). Resting sarcomere length was $1.90 \pm 0.01 \mu\text{m}$ for the LV cells versus $1.89 \pm 0.01 \mu\text{m}$ for the RV cells ($P = \text{NS}$). Statistical comparisons are by two-way ANOVA and a means comparison contrast (33), where $n =$ number of cells. $*P < 0.001$ for difference from the LV value at matched time points; $\dagger P < 0.001$ for difference from the initial time 0 value within a group.

issues to be resolved. (i) The increased microtubules in stress-hypertrophied cardiocytes may be the direct result of mechanical load, but additional or alternative mechanisms such as posttranslational modifications of tubulin (26) or increased microtubule-associated proteins (27), each of which enhances microtubule stability, may be operative. (ii) The increased free RV tubulin seen in the immunoblots (Fig. 1) for the PAB cats was unexpected in view of the negative feedback control of tubulin synthesis (28). Thus, tubulin synthesis and its assembly into microtubules needs to be investigated in the stress-hypertrophied car-

diocyte. (iii) The contractile defect described here at the cellular level needs to be studied at the tissue level, especially in the pressure-overloaded left ventricle where the great preponderance of clinically significant human pathophysiology occurs.

REFERENCES AND NOTES

- G. Cooper, *Annu. Rev. Physiol.* **49**, 501 (1987).
- _____, F. J. Puga, K. J. Zujko, C. E. Harrison, H. N. Coleman, *Circ. Res.* **32**, 140 (1973).
- G. Cooper, R. M. Satava, C. E. Harrison, H. N. Coleman, *ibid.* **33**, 213 (1973).
- D. L. Mann, Y. Urabe, R. L. Kent, S. Vinciguerra, G. Cooper, *ibid.* **68**, 402 (1991).
- D. W. Sack, G. Cooper, C. E. Harrison, *Basic Res. Cardiol.* **72**, 268 (1977).
- P. Nick, E. Schäfer, R. Hertel, M. Furuya, *Plant Cell Physiol.* **32**, 873 (1991).
- S. Caveney, *J. Cell Sci.* **4**, 541 (1969).
- C. L. Ives, S. G. Eskin, L. V. McIntire, *In Vitro Cell. Dev. Biol.* **22**, 500 (1986).
- T. L. Hill and M. W. Kirschner, *Int. Rev. Cytol.* **78**, 1 (1982).
- T. J. Dennerll, H. C. Joshi, V. L. Steel, R. E. Buxbaum, S. R. Heidemann, *J. Cell Biol.* **107**, 665 (1988).
- T. A. Marino *et al.*, *Am. J. Physiol.* **249**, H371 (1985).
- M. A. Goldstein and M. L. Entman, *J. Cell Biol.* **80**, 183 (1979).
- Right Ventricular volume overload in the ASD group was produced (2) by partial resection of the interatrial septum during venous inflow occlusion. RV pressure overload in the PAB group was produced (3) by placement of a 3.5-mm inside diameter band around the proximal pulmonary artery. Because the RV mass increase stabilizes by 2 weeks after a step increase in load [A. L. Bassett and H. Gelband, *Circ. Res.* **32**, 15 (1973)], at 2 weeks, 4 weeks, or later times after surgery intravascular pressures and oxygen saturations were measured (4); values in the systemic circulation were the same for all groups. The heart was removed, RV mass was determined, and Ca^{2+} -tolerant quiescent cardiocytes were isolated enzymatically (4, 29) from the RV and LV separately. All operative procedures were carried out under full surgical anesthesia with ketamine HCl [50 mg per kilogram of body mass, intramuscularly (i.m.)], meperidine (2.2 mg/kg, i.m.), and acepromazine maleate (0.25 mg/kg, i.m.). All procedures and the care of the cats were in accordance with institutional guidelines.
- Cardiocyte surface area was obtained [D. L. Mann, R. L. Kent, G. Cooper, *Circ. Res.* **64**, 1079 (1989)] from digitized photographs both of a random sampling of cells from each cat and of each cell in which contractile function was characterized; this dimension did not differ in the two groups of cells. The data given (Table 1) are for the combined samples and were gathered from 142 cells in the control cats, from 94 cells in the ASD cats, and from 553 cells in the PAB cats.
- H. Tsutsui, K. Ishihara, G. Cooper, unpublished data.
- I. Klein, *Cardiovasc. Res.* **17**, 459 (1983).
- T. J. Lampidis, K. W. Trevorrow, R. W. Rubin, *Exp. Cell Res.* **164**, 463 (1986).
- R. E. Ostlund, J. T. Leung, S. V. Hajek, *J. Cell Biol.* **85**, 386 (1980).
- P. B. Schiff, J. Fant, S. B. Horwitz, *Nature* **277**, 665 (1979).
- O. J. Itoh and H. Sato, *Biochim. Biophys. Acta* **800**, 21 (1984).
- I. Virtanen, V. P. Lehto, E. Lehtonen, *Eur. J. Cell Biol.* **23**, 80 (1980).
- A. F. Miranda and G. C. Godman, *Tissue Cell* **5**, 1 (1973).
- H. Tsutsui, R. L. Kent, M. Nagatsu, K. Ishihara, G. Cooper, *Circulation* **86** (suppl. 1), I-5 (1992).
- L. Rappaport and J. L. Samuel, *Int. Rev. Cytol.* **113**, 101 (1988).
- J. Schaper *et al.*, *Circulation* **83**, 504 (1991).
- G. Gundersen, S. Khawaja, J. C. Bulinski, *J. Cell Biol.* **109**, 2275 (1989).
- J. B. Olmsted, *Annu. Rev. Cell Biol.* **2**, 421 (1986).
- T. J. Yen, P. S. Machlin, D. W. Cleveland, *Nature* **334**, 580 (1988).
- G. Cooper *et al.*, *Circ. Res.* **58**, 692 (1986).
- R. E. Ostlund, J. T. Leung, S. V. Hajek, *Anal. Biochem.* **96**, 155 (1979).
- For the immunoblot analysis, fresh 0.5-g specimens from the RV and LV of each of the four indicated types of cats were homogenized in 5 ml of microtubule stabilizing buffer (30) and centrifuged at 100,000g (15 min, 25°C). The supernatants were saved as the free tubulin fractions, and the pellets were resuspended at 0°C in 4 ml of microtubule depolymerization buffer (30); after 1 hour they were centrifuged at 100,000g (15 min, 4°C), and the supernatants were saved as the polymerized tubulin fractions. Protease inhibitors [D. G. Drubin, S. C. Feinstein, E. M. Shooter, M. W. Kirschner, *J. Cell Biol.* **101**, 1799 (1985)] were used throughout. For the subsequent 8 to 16% gradient SDS-polyacrylamide gel electrophoresis analysis, equal proportions of the free and polymerized samples were loaded onto the two lanes for each ventricle, and an equal amount of protein as determined by a bicinchoninic acid assay (BCA, Pierce) was loaded for the RV and LV samples. The samples were then transferred to polyvinylidene difluoride membranes (35 V, 75 min) and probed with a 1:5000 dilution of a monoclonal antibody to β -tubulin (DM1B; Amersham). The bound antibody was visualized with a horseradish peroxidase-conjugated secondary antibody (Vector) and enhanced chemiluminescence (ECL, Amersham). No β -tubulin was detectable in the supernatant when the initial pellets were re-extracted in stabilizing buffer. In all cases, a single band at 55 kD having the same mobility as concurrently run bovine brain β -tubulin was detected. When 0.5-g RV and LV specimens were initially homogenized in depolymerization buffer (30) to isolate total tubulin, the RV and LV values were the same in control and ASD cats, but the RV value was double the LV value in 2-week and 4-week PAB cats (15). For the indirect immunofluorescence micrographs, freshly isolated (4, 29) RV and LV cardiocytes were permeabilized for 1 min by 1% Triton X-100 in stabilization buffer [M. Schliwa, J. van Blerkom, K. R. Porter, *Proc. Natl. Acad. Sci. U.S.A.* **78**, 4329 (1981)], washed twice in the same buffer, cytosol onto cover slips at 500g for 15 min, and fixed for 10 min with 3.7% formaldehyde. After blocking with 10% horse serum in 0.1 M glycine, the cells were incubated overnight at 4°C with a 1:1000 dilution of the same antibody to β -tubulin used for the immunoblots, followed by a fluorescein-conjugated secondary antibody (Vector). The cells were mounted with 1% triethylenediamine and 50% glycerol in phosphate-buffered saline, and 0.7- μ m optical sections were obtained by confocal laser microscopy (LSM GB-200, Olympus).
- The techniques used to measure sarcomere motion in isolated cardiocytes have been described [R. L. Kent *et al.*, *Am. J. Physiol.* **257**, H1717 (1989)]. The cells were studied at $37.0 \pm 0.1^\circ\text{C}$ while stimulated at 0.25 Hz. To characterize the effects of microtubule depolymerization, colchicine at a final concentration of 10^{-6} M was added to the chamber containing the cardiocytes, and the contractile function of the same single cell was followed over the ensuing hour. A dose-response curve had shown that 10^{-6} M colchicine had a maximum effect on the extent and velocity of sarcomere shortening, and lumicolchicine (10^{-5} M), the inactive stereoisomer of colchicine, was without effect on any aspect of sarcomere mechanics in RV or LV cardiocytes from PAB cats; immunoblot analysis of free and polymerized tubulin and immunofluorescence of isolated cardiocytes, with the use of the methods described (Fig. 1), had shown a complete absence of microtubules after treatment with 10^{-6} M colchicine for

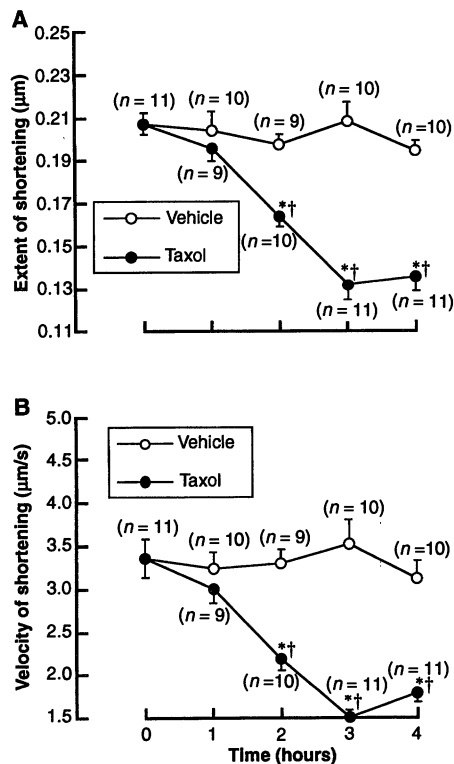


Fig. 5. Effects of taxol on the maximum extent (A) and velocity (B) of sarcomere shortening in cardiocytes isolated from normal cats; the same cells are characterized in both panels. For the vehicle group, the superfusate consisted of the buffer (Fig. 2) to which 10^{-4} M dimethyl sulfoxide had been added. For the taxol group, the superfusate consisted of the same buffer to which 10^{-4} M dimethyl sulfoxide and 10^{-5} M taxol had been added. The time (in hours) after the addition of taxol is indicated. Immunoblot analysis of free and polymerized tubulin and immunofluorescence micrograph analysis of microtubules in isolated cardiocytes, with the methods described (Fig. 1), demonstrated an increase in polymerized β -tubulin on exposure to 10^{-5} M taxol for 3 hours (15). Resting sarcomere length was 1.94 ± 0.02 μm . Statistical comparisons are by two-way ANOVA and a means comparison contrast (33), where n = number of cells. $*P < 0.001$ for difference from the vehicle value at matched time points; $\dagger P < 0.001$ for difference from the initial time 0 value within a group.

1 hour (15). Examination of these cells when loaded with fluo-3 after exposure to 10^{-6} M colchicine for 1 hour did not show an increase in the concentration of intracellular Ca^{2+} in either contracting or quiescent cardiocytes (15).

33. R. R. Hocking, *The Analysis of Linear Models* (Brooks-Cole, Monterey, CA, 1985), pp. 69–101.

34. We thank S. Prutting, V. Harper, and M. Barnes for technical assistance and J. Lindroth for computer programming. Supported by the Veterans Administration and by the NIH (grant HL37196). G.C. is a VA Clinical Investigator.

29 October 1992; accepted 26 February 1993

Intermediate Filament Formation by a Yeast Protein Essential for Organelle Inheritance

Stephen J. McConnell and Michael P. Yaffe*

Intermediate filaments are abundant cytoskeletal components whose specific cellular functions are poorly understood. The *Saccharomyces cerevisiae* protein MDM1 displays structure and solubility properties that are similar to those of intermediate filament proteins of animal cells. Yeast cells that have a mutant form of MDM1 exhibit temperature-sensitive growth and defective transfer of nuclei and mitochondria to daughter cells during incubation at the nonpermissive temperature of 37°C. The purified, wild-type MDM1 protein readily forms 10-nanometer-wide filaments at either 4°C or 37°C. In contrast, the purified, mutant protein forms filaments at 4°C but fails to form such structures at 37°C. These results suggest that intermediate filament proteins are universal components of eukaryotic cells.

Intermediate filaments have been characterized extensively in higher eukaryotic cells and constitute a prominent system of filaments, 10 nm in diameter, that extend in arrays and networks throughout the cytoplasm (1, 2). The proteins that form these networks share certain conserved structural features and physical properties (3–5). In addition, purified intermediate filament proteins from a number of sources are able to self-assemble into 10-nm-diameter filaments in vitro in a process independent of energy requirements or cofactors (5). Cytoplasmic intermediate filaments have been implicated in a number of roles, including maintaining cellular mechanical stability (6) and mediating intracellular communication (2), although many details of their dynamics and specific cellular functions are obscure (1, 2, 5).

The yeast MDM1 protein shares several properties with intermediate filament proteins of animal cells, including a similar solubility profile and similarities of amino acid sequence (7). MDM1 was identified through the analysis of a *Saccharomyces cerevisiae* mutant, *mdm1*, that displays temperature-sensitive growth and a failure to transfer nuclei and mitochondria into developing daughter buds during incubation at 37°C (8). The wild-type MDM1 gene was cloned, and its product (MDM1) was shown to be an essential, 51-kD polypeptide (7). Antibodies raised against MDM1 recognized a pattern of spots and punctate arrays distributed throughout the yeast cell

cytoplasm. In *mdm1* mutant cells, these structures were apparent at 4°C and 23°C but disappeared after *mdm1* mutant cells were shifted to the nonpermissive temperature (7). Affinity-purified antibodies against MDM1 also recognized intermediate filaments in indirect immunofluorescence of a variety of animal cells (7).

To compare wild-type and mutant forms of MDM1, we cloned and analyzed the mutant gene (9). The *mdm1* gene was isolated from mutant yeast by the allelic-marker rescue approach (10). The identity of the recovered gene was confirmed by nucleotide sequence analysis (11), which revealed a single difference from the wild-type gene: a transition of G to A at nucleotide 770, resulting in a change of Ser²⁵⁷ to Asn. When a wild-type copy of MDM1 was replaced by the recovered mutant *mdm1* gene in intact cells, the original mutant phenotype was generated (12).

Both wild-type and mutant MDM1 proteins were produced for further analysis by expression of the genes in bacterial cells (13) (Fig. 1A). Purification of wild-type and mutant proteins from bacterial inclusion bodies by differential extraction (14) yielded essentially homogeneous preparations (Fig. 1B).

To test the ability of MDM1 to self-assemble into filaments, we dialyzed the purified protein solubilized in 9 M urea against buffers of physiological or low ionic strength (15). Protein samples then were examined by electron microscopy on grids after negative staining. Wild-type MDM1 protein readily formed filaments during dialysis against a physiological salt solution (Fig. 2, A through C). Filaments displayed

a generally curvilinear, "smooth" appearance (Fig. 2, A through C), with an average diameter of 10.12 ± 0.45 nm ($n = 50$). Tangled or aggregated filamentous structures were also apparent on the grids (Fig. 2B). Under the conditions used for filament assembly, 20 to 40% of the purified MDM1 appeared competent for incorporation into filaments or filamentous structures (16). Filaments recovered by centrifugation after dialysis or generated by several cycles of solubilization in 9 M urea, reformation by dialysis, and recovery by centrifugation had the same appearance (12). Dialysis of urea-solubilized samples at various protein concentrations indicated that MDM1 displays a critical concentration for filament assembly of approximately 50 μ g/ml. Individual filaments or filamentous aggregates failed to form upon dialysis of MDM1 against a buffer of low ionic strength (Fig. 2D). These results demonstrate that the MDM1 protein can self-assemble into 10-nm-wide filaments in the absence of high-energy compounds or other cofactors.

The wild-type MDM1 protein was found to form filaments during dialysis at either 4°C (Fig. 3A) or 37°C (Fig. 3B). Filaments assembled at either temperature appeared equivalent and formed with approximately the same critical concentration for assembly. The purified, mutant MDM1 protein, encoded by the *mdm1* gene, also formed 10-nm-wide filaments at 4°C (Fig. 3C). These filaments were essentially identical to those formed by the wild-type protein. The

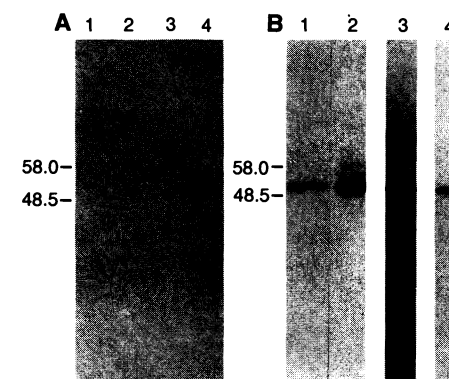


Fig. 1. Expression and purification of MDM1. (A) Immunoblot of MDM1 in protein extracts of bacterial cells that had a control vector, pET11-a (lanes 1 and 2), or a vector encoding MDM1, pET11-a-MDM1 (lanes 3 and 4). Cells were uninduced (lanes 1 and 3) or induced with isopropyl-1-thio- β -D-galactoside (lanes 2 and 4). (B) Analysis of purified MDM1. Lane 1, wild-type MDM1 protein (5 μ g) stained with Coomassie blue; lane 2, wild-type MDM1 protein (30 μ g) stained with Coomassie blue; lane 3, mutant MDM1 protein (7 μ g) stained with Coomassie blue; lane 4, immunoblot analysis of wild-type MDM1 (100 ng). Molecular size markers are indicated to the left of (A) and (B) in kilodaltons.

Department of Biology, University of California at San Diego, La Jolla, CA 92093.

*To whom correspondence should be addressed.